IAC-04-A.4.10

INTERNATIONAL SPACE STATION LEAK LOCALIZATION USING VENT TORQUE ESTIMATION

Jong-Woo Kim, John L. Crassidis
Department of Mechanical and Aerospace Engineering
University at Buffalo, The State University of New York
Amherst, NY 14260-4400
716-645-2593 ext. 2246
boungdong@yahoo.com, johnc@eng.buffalo.edu

Srinivas R. Vadali
Department of Aerospace Engineering
Texas A&M University
College Station, TX 77843-3141
979-845-6051
svadali@aero.tamu.edu

Adam L. Dershowitz
United Space Alliance
NASA Johnson Space Center, Code DF64
Houston, TX 77058
281-483-5410
dersh@alum.mit.edu

ABSTRACT

A new method is presented in this paper to localize air leaks on the International Space Station based on the spacecraft attitude and rate behavior produced by a mass expulsion force of the leaking air. Thrust arising from the leak generates a disturbance torque, which is estimated using an unscented filter with a dynamical model (including external disturbances such as aerodynamic drag and gravity-gradient). The leak location can be found by estimating the moment arm of the estimated disturbance torque, assuming that leak is caused by only one hole. Knowledge of the leak thrust magnitude and its resulting disturbance torque are needed to estimate the moment arm. The leak thrust direction is assumed to be perpendicular to the structure surface and its magnitude is determined using a Kalman filter with a nozzle dynamics model. There may be multiple leak locations for a given response, but the actual geometric structure of the space station eliminates many of the possible solutions. Numerical results show that the leak localization method is very efficient when used with the conventional sequential hatch closure or airflow induction sensor system. A user friendly computer code has been developed to find the leak location with the proposed method.

INTRODUCTION

The International Space Station (ISS) is orbiting in a 51.6° inclination near-circular Low-Earth-Orbit (LEO) with an altitude between 370 and 460 km, and is expected to have a minimum operational lifetime of 15 years. Because of the large structure, long lifetime and orbit characteristics,[1] the ISS may be subject to impacts of hyper velocity particles such as micro-meteorites and space debris that can severely damage the station. This damage may threaten the safety of the crew if the pressurized wall of a module is perforated, which may result in significant air loss. Collisions with other objects are another possible cause of a leak, as occurred in the Russian Space Station Mir in 1997. To protect the ISS from the impact damages, various debris shields have been designed. Heavy shields are placed in the forward facing area which is likely to be

hit frequently, and fewer shields are used in the nadir-facing and aft area.[2]

Perforations in a pressurized module will result in a rapid temperature and pressure decrease. Therefore fast determination of the extent and location of the leak is needed to maintain the operational status in order to provide safety for the crew. The first indication of a leak in the ISS is the depressurization of a module. The leak size can be calculated by measuring the internal pressure and its depressurization rate. Based on the extent of leak it is possible to calculate the "reserve time" left until a crew evacuation is required. Depending on the reserve time operational decisions must be made, including: 1) whether or not to perform a leak isolation to patch the leak, or 2) evacuate the ISS. Leak localization should be performed first to find the leaking module. Then the exact location within the leaking module for repair purposes can be determined.

Conventional methods to locate air leaks on the ISS include the sequential module leak isolation process for the US segment (prior to assembly stage 10A) and the airflow induction sensor system for the Russian segment. The sequential module leak isolation process involves having the crew close hatches sequentially while monitoring the pressure difference across each hatch. A drawback of this process is very small pressure differences can keep a closed hatch from being open again, which significantly reduces the reserve time and can pose an immediate risk to the crew. Thus, safety dictates that the hatches be closed in an order that will never trap a crew member away from the escape vehicle. This may significantly inhibit the leak isolation process if the leaking module is not located within the first few hatch closures.

The airflow induction sensor system employs hot-wire anenometers situated in hatchways to measure the air flow direction and its rate. The hot-wire anenometer operates by air passing across a wire with a current running through it to maintain a constant temperature in the wire. These devices are installed at all hatchways of the Russian segments. However, the airflow induction sensor system designed for the ISS has several limitations for the following reasons. The sensors are not mounted at all hatchways of the US segment (only at Node-2 and Node-3 of the US segment). Therefore the sequential module isolation process is still needed to determine which module leaks in the US segments. Since the sensors are very sensitive to the air circulation inside, the venting system and the movement of the crew must be stopped for several minutes, which may waste time in an emergency situation. Because these sensors are situated in hatchways, the location of the leak within the suspected leaking module cannot be found for repair purposes without using other inspection processes (this is also true for the sequential isolation process). Therefore a more efficient localization system is needed to locate the leaks.

The new method presented in this paper uses the attitude response of the ISS caused by the leak reaction force of the air flowing through a perforated hole. The vent thrust can yield a strong reaction torque depending on the size and location of the leak. A leak hole on the surface of a pressurized module can be modeled as a short nozzle with the leaking air as the propellant. We assume that the line of action of the vent thrust is perpendicular to the cross section area of the leak hole. This assumption is reasonable due to the relatively thin skin of each module. Based on the nozzle dynamics, an extended Kalman filter (EKF) algorithm is used to estimate the vent thrust magnitude with the internal pressure measurements. The venting torque is estimated by the Unscented Filter (UF) developed by Julier and Uhlman.[3] The advantages of the UF are: 1) it captures the posterior mean and covariance of a random variable accurately to the second-order Taylor series expansion for any nonlinearity by choosing a minimal set of sample points and propagating them through the original nonlinear system, 2) it is derivative-free when the filter equations are already expressed in discrete forms, i.e. no Jacobian and Hessian calculations need to be evaluated for the computation which enable the UF to be applied to any complex dynamical system and to non-differentiable functions.[4] The vent torque, which is not explicitly modeled in the attitude dynamics, shows up as a residual disturbance torque when the spacecraft angular rate measurement undergoes a filtering process. In the disturbance torque estimation algorithm, the filter state vector is augmented to include the unknown parameters as additional states, resulting in a total of six states, where three states are for the total angular momentum of the spacecraft and the remaining three states are for the 3-axis components of the disturbance torque. But problems arise when the unmodeled dynamics (besides the vent torque) dominate the residual torque.

Among the external disturbances, the aerodynamic torque is known to have large uncertainties in its parameters but has relatively less effects on the residual disturbance torque estimation results compared to the uncertainties in the inertia components of the ISS. Therefore parameter estimation methods is employed to estimate the six inertia components when we know that there is not a venting leak acting on the spacecraft. The UF algorithm is employed to estimate the inertia in real time. It is shown that the complete inertia parameters are unobservable when the space station attitude is in its torque equilibrium attitude (TEA), which is the nominal ISS operational attitude. But the inertia observability can be strengthened with the presence of attitude maneuvers. Problems in estimating uncertain inertia and external disturbance torque for the ISS are investigated in several papers such as Refs. 5 and 6. In Ref. 7, small sinusoidal probing signals are used to enhance the observability of the inertia by causing attitude motion about the TEA. Also in Ref. 6, the estimation algorithm to determine the mass and aerodynamic torque properties of the ISS in Low-Earth Orbit (LEO) based on the least-square method has been derived with the use of an indirect adaptive control algorithm to enhance the observability of the unknown parameters. This method uses a smoothing method to estimate the unmeasured angular acceleration.

The possible locations of the air leak are then calculated

using the estimated vent torque, vent thrust magnitude, and the actual geometric structure of the pressurized segments. For simplicity, the disturbance torque caused by the pressure of the impingement of the leaking air plume on nearby surfaces is neglected. Also, we assume that the leak is caused by a single leak hole. There may be single or multiple leak locations that produce the same attitude response. To reduce the number of possible solutions, conventional methods are combined with the new leak localization method. This approach reduces the number of possible solutions, so that fewer hatch closures are required to uniquely determine the leak location. Advantages of the attitude response method include:

1. No other devices are needed besides pressure gauges to measure the air pressure, and spacecraft attitude and rate sensors.

2. Relatively fast leak localization can be achieved compared to the conventional leak localization method proposed for the ISS.

3. The new method not only determines the possible leaking modules but also determines the possible locations of the leak hole within those modules. This may be critical to allow for repairs rather than sealing off a module or performing a station evacuation.

The remainder of paper is organized as follows. First, a summary of the attitude dynamics for the ISS is given. Next, using the isentropic nozzle theory, the vent thrust is calculated using the isentropic and isothermal air depressurization models. Then a brief explanation on UF is given with the derivations of disturbance torque estimation. Then we describe the steps to locate leak once we know the disturbance torque and the thrust due to a leak. Finally numerical simulations for the leak localization are presented with conclusions.

SPACECRAFT ATTITUDE DYNAMICS

The dynamic equations of rotational motion of a rigid spacecraft in a LEO environment are given by Euler's equation:

$$\dot{\boldsymbol{H}} = -\left[J^{-1}\left(\boldsymbol{H}-\boldsymbol{h}\right)\right]\times\boldsymbol{H}+\boldsymbol{N}_{drag}+\boldsymbol{N}_{grav}+\boldsymbol{d}_{vent} \tag{1}$$

where $\mathbf{H}$ is the total angular momentum of the spacecraft satisfying

$$\boldsymbol{H} = J\boldsymbol{\omega}+\boldsymbol{h} \tag{2}$$

and J is the inertia matrix, $\boldsymbol{N}_{drag}$ is the aerodynamic torque, $\boldsymbol{N}_{grav}$ is the gravity gradient torque, $\boldsymbol{h}$ is the angular momentum of the control moment gyroscopes (CMGs), and $\boldsymbol{d}_{vent}$ is the torque due to a vent. Other environmental effects such as solar radiation and Earth's albedo are neglected. The effects caused by solar arrays rotations are omitted since they have little effects on the attitude dynamics but note that the resultant aerodynamic torques produced by the arrays rotations may be significant.

The gravity-gradient torque for a circular orbiting spacecraft is given by

$$\boldsymbol{N}_{grav} = 3n^2\mathbf{C}_3\times J\,\mathbf{C}_3 \tag{3}$$

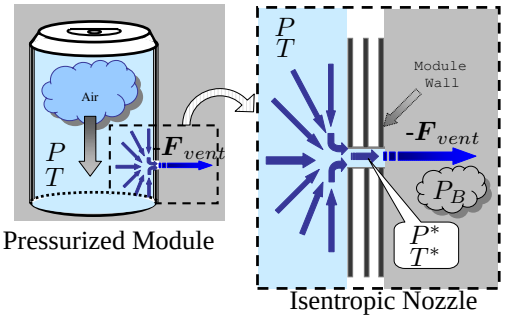

Fig. 1 Air Flow Through Leak Hole

where $\mathbf{C}_i$ is the i^{th} column of the coordinate transformation matrix from the LVLH orbital reference frame to the body reference frame, and n is the time-varying orbital frequency calculated from orbital elements of the spacecraft.

The aerodynamic torque $\boldsymbol{N}_{drag}$ is modelled such that the drag force and the center of pressure location are functions of the attitude of the spacecraft:

$$\boldsymbol{N}_{drag} = -\frac{1}{2}\rho_a v_a^2 C_D S\left[\boldsymbol{\rho}_{cp}\times\mathbf{C}_1(\boldsymbol{q})\right] \tag{4}$$

where v_a is the magnitude of the atmospheric velocity with respect to the spacecraft, which can be approximated as the circular orbital speed. The atmospheric density ρ_a is calculated using Marshall Engineering Thermosphere (MET) model which accounts the seasonal and diurnal heating effects of the Earth's atmosphere. The drag coefficient C_D is assumed to be constant for a given orientation of the spacecraft. Also, S is the attitude dependent frontal area and $\boldsymbol{\rho}_{cp}$ is the attitude dependent center of pressure location. The attitude dependent aerodynamic parameters are calculated with the method developed in 8, where the reference area and the center of pressure are calculated for any orientation by defining interpolation functions. The projected area and the center of pressure for the three orthogonal body reference axes of the ISS are given in 1 for each assembly stage.

The vent torque is modelled by

$$\boldsymbol{d}_{vent} = \boldsymbol{r}_{vent}\times\boldsymbol{F}_{vent} \tag{5}$$

where $\boldsymbol{r}_{vent}$ is the moment arm of a vent torque from the center of mass of the spacecraft to a leak location, and $\boldsymbol{F}_{vent}$ is a vent thrust. The vent torque is unknown and will be estimated by treating it as a state in the real-time filter algorithm.

VENT THRUST

A leak hole perforated on the surface of a pressurized module will behave like a short length nozzle. The dynamic properties of the air flow through the leak hole are analyzed using one dimensional isentropic and isothermal nozzle dynamic models. Fig. 1 shows the diagram of the air flow through the leak hole on the pressurized module, where T^* and P^* are the temperature and pressure of the

air in the leak hole, respectively, T and P are the temperature and pressure of the inside of the pressurized module, respectively, $\boldsymbol{F}_{vent}$ is the vent thrust, and P_B is the back pressure. The mass flow rate in a leak hole is given by[9]

$$\dot{m} = -\frac{AP^*v^*}{RT^*} \tag{6}$$

where A is the area of the hole, R is the ideal gas constant (287 N-m/Kg-K), and v^* is the exhaust velocity of the air satisfying

$$v^* = \sqrt{\gamma RT^*} \tag{7}$$

where γ is the specific heat ratio, with $\gamma = 1.4$ for an ideal gas. The mass flow rate $\dot{m}$ can be expressed as a function of the air inside the pressurized module. This is accomplished by substituting the following expressions into Eq. (6):

$$P^* = P\left(\frac{2}{\gamma+1}\right)^{\frac{\gamma}{\gamma-1}} \tag{8a}$$

$$T^* = T\left(\frac{2}{\gamma+1}\right) \tag{8b}$$

yielding

$$\dot{m} = -\frac{AP\sqrt{\gamma}}{\sqrt{RT}}\left(\frac{2}{1+\gamma}\right)^{\frac{1+\gamma}{2(\gamma-1)}} \tag{9}$$

The actual mass flow rate can be calculated by multiplying $\dot{m}$ in Eq. (6) by the discharge coefficient C_D. Using the thrust equation the vent thrust magnitude is given by

$$|\boldsymbol{F}_{vent}| = C_D\dot{m}v^* + (P^* - P_a)A \tag{10}$$

where P_a is the ambient pressure which is approximately zero for the vacuum of space. Substituting Eqs. (6), (7) and (8) into Eq. (10), and simplifying yields

$$|\boldsymbol{F}_{vent}| = AP\left(C_D\gamma + 1\right)\left(\frac{2}{\gamma+1}\right)^{\frac{\gamma}{\gamma-1}} \tag{11}$$

Note that the magnitude of the vent thrust is proportional to the pressure inside the module and to the area of the leak hole. This expression is very useful since the vent thrust magnitude is a direct function of the internal pressure P, which can be measured by a pressure sensor. For the calculation of the hole area A the following approach is used. The indication of an air leak in a pressurized module is the depressurization of the air. The air inside the module follows the ideal gas law, given by

$$P = \frac{mRT}{V} \tag{12}$$

where V is the volume of the air. Differentiating Eq. (12) with respect to time and using $\dot{m}$ from Eq. (9) gives a depress rate model. Two kinds of depressurization process models are used, depending on the temperature characteristics of the air. For an isentropic air model, where P and T is related by

$$T = T_0\left(\frac{P}{P_0}\right)^{\frac{\gamma-1}{\gamma}} \tag{13}$$

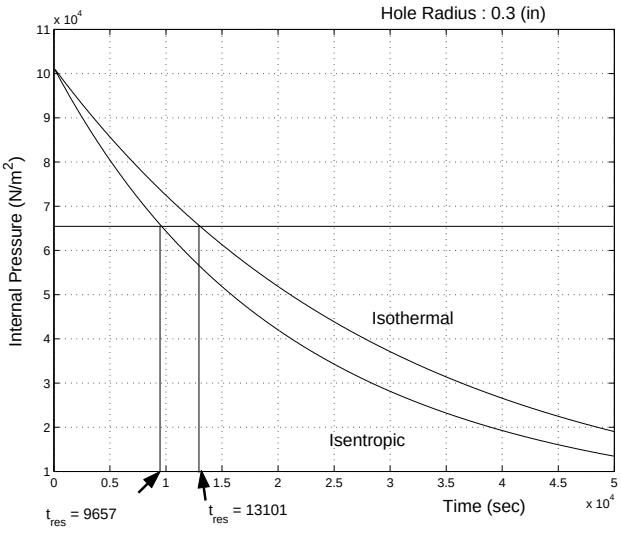

Fig. 2 Internal Pressure

the depressurization rate $\dot{P}$ is

$$\dot{P} = -k_1AP^{k_2} \tag{14a}$$

$$k_1 = \frac{\gamma\sqrt{RT_0\gamma}}{V}P_0^{\frac{1-\gamma}{2\gamma}}\left(\frac{2}{\gamma+1}\right)^{\frac{\gamma+1}{2(\gamma-1)}}C_D \tag{14b}$$

$$k_2 = \frac{3\gamma-1}{2\gamma} \tag{14c}$$

For an isothermal process, T is treated as a constant in Eq. (12). Therefore the depressurization rate $\dot{P}$ can be derived as

$$\dot{P} = -k_3AP_0 \tag{15a}$$

$$k_3 = \frac{\sqrt{RT_0\gamma}}{V}\left(\frac{2}{1+\gamma}\right)^{\frac{1+\gamma}{2(\gamma-1)}}C_D \tag{15b}$$

where the subscript 0 stands for the initial value and, k_1, k_2 and k_3 are constants. Now, we can calculate the hole area A by measuring the internal pressure P and its depress rate $\dot{P}$.

Comparisons between the isentropic and isothermal gas model are shown in Figs. 2 and 3, using the ISS assembly Stage 16A with a leak hole radius of 0.3 inch. From Fig. 2, the isentropic gas model gives a faster pressure drop in the internal pressure than the isothermal gas model. Therefore the reserve time t_{res}, which is a measure of the time it takes for the current pressure P to reach the minimum habitable pressure $P_{min} \approx 490$ mmHg, is shorter using the isentropic gas model than using the isothermal gas model. The reserve time t_{res} can be obtained by integrating Eq. (14b) for the isentropic process and Eq. (15a) for the isothermal process. The reserve time for the isentropic process is

$$t_{res} = \frac{\left(\frac{P_{min}}{P}\right)^{\frac{1-\gamma}{2\gamma}} - 1}{\frac{\gamma-1}{2}\frac{A}{V}\sqrt{RT\gamma}\left(\frac{2}{\gamma+1}\right)^{\frac{\gamma+1}{2(\gamma-1)}}C_D} \tag{16}$$

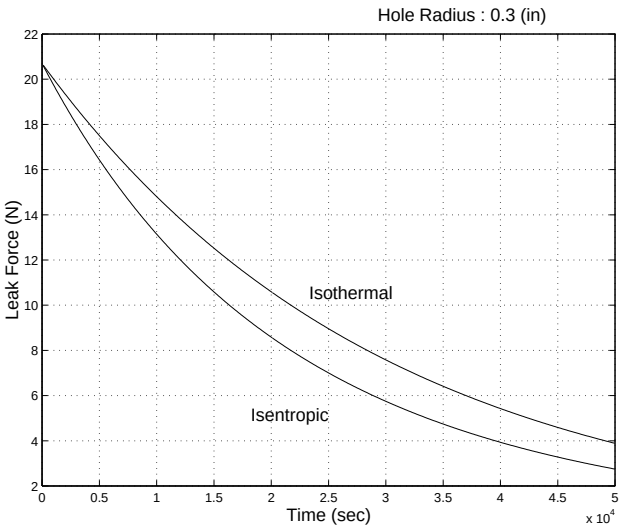

Fig. 3 Vent Thrust Magnitude

where the internal temperature T can be substituted by P from Eq. (13). From Fig. 3 the vent thrust magnitude is larger using the isothermal gas model, meaning the isothermal gas model produces a greater torque than the isentropic gas model. If the leak area hole size is small then the isothermal model can be used (since the temperature will remain fairly constant), otherwise the isentropic model should be used.

VENT THRUST ESTIMATION

Since the actual internal pressure measurements are corrupted by noise, the Kalman filter is used to estimate the hole area which is needed to calculate the magnitude of vent thrust with Eq. (11). The state equations for the depressurization process have the following form

$$\dot{\boldsymbol{x}}(t) = \boldsymbol{f}\left[\boldsymbol{x}(t), t\right] + \boldsymbol{\eta}(t) \tag{17}$$

where the state $\boldsymbol{x}(t) = [P(t),\ A(t)]^T$ and

$$\boldsymbol{f}\left[\boldsymbol{x}(t), t\right] = \begin{bmatrix} -k_1 A P^{k_2} \\ 0 \end{bmatrix} \tag{18}$$

for an isentropic process model, and

$$\boldsymbol{f}\left[\boldsymbol{x}(t), t\right] = \begin{bmatrix} -k_3 A P \\ 0 \end{bmatrix} \tag{19}$$

for isothermal process model. The vector $\boldsymbol{\eta} = [\eta_1,\ \eta_2]^T$ is the process noise vector, where η_1 and η_2 are Gaussian white-noise processes with

$$E\left\{\eta_i(t)\right\} = 0 \tag{20a}$$
$$E\left\{\eta_i(t)\eta_j(t')\right\} = Q_i \delta_{i,j}(t - t') \tag{20b}$$

with $i,\ j = 1,\ 2$. The matrix Q_i has the following form

$$Q = \begin{bmatrix} \sigma_1^2 & 0 \\ 0 & \sigma_2^2 \end{bmatrix} \tag{21}$$

where the terms σ_1^2 and σ_2^2 are the variances of η_1 and η_2, respectively. The internal pressure measurement is modelled as

$$\tilde{z}_k = h_k\left[\boldsymbol{x}(t_k)\right] + v_k, \quad k = 1,\ 2,\ \ldots,\ m \tag{22a}$$
$$h_k\left[\boldsymbol{x}(t_k)\right] = P_k, \quad k = 1,\ 2,\ \ldots,\ m \tag{22b}$$

where m is the number of measurements and v_k is the measurement noise which satisfies a discrete Gaussian white-noise process with

$$E\left\{v_k\right\} = 0 \tag{23a}$$
$$E\left\{v_k v_{k'}\right\} = R_k \delta_{k,k'} \tag{23b}$$

The propagation of the state satisfies

$$\dot{\hat{\boldsymbol{x}}}(t) = \boldsymbol{f}\left[\hat{\boldsymbol{x}}(t), t\right] \tag{24a}$$
$$\hat{z}_k = h_k\left[\hat{\boldsymbol{x}}(t_k)\right] \tag{24b}$$

where $\hat{\boldsymbol{x}}(t) = [\hat{P}(t),\ \hat{A}(t)]^T$ is the state estimate vector. The error covariance propagation matrix $\mathcal{P}$ satisfies

$$\dot{\mathcal{P}}(t) = F\left[\hat{\boldsymbol{x}}(t), t\right]\mathcal{P}(t) + \mathcal{P}(t)F\left[\hat{\mathbf{x}}(t), t\right]^T + Q \tag{25}$$

where $F\left[\hat{\boldsymbol{x}}(t), t\right]$ is given by

$$F\left[\hat{\boldsymbol{x}}(t), t\right] = \left.\frac{\partial \boldsymbol{f}\left[\boldsymbol{x}(t), t\right]}{\partial \boldsymbol{x}(t)}\right|_{\boldsymbol{x}=\hat{\boldsymbol{x}}} \tag{26a}$$
$$= \begin{bmatrix} -k_1 k_2 \hat{A}\hat{P}^{k_2 - 1} & -k_1 \hat{P}^{k_2} \\ 0 & 0 \end{bmatrix} \tag{26b}$$

for an isentropic process, and

$$F\left[\hat{\boldsymbol{x}}(t), t\right] = \left.\frac{\partial \boldsymbol{f}\left[\boldsymbol{x}(t), t\right]}{\partial \boldsymbol{x}(t)}\right|_{\boldsymbol{x}=\hat{\boldsymbol{x}}} \tag{27a}$$
$$= \begin{bmatrix} -k_3 \hat{A} & -k_1 \hat{P} \\ 0 & 0 \end{bmatrix} \tag{27b}$$

for an isothermal process.

The state estimate and error covariance updates are given by

$$\hat{\boldsymbol{x}}_k^+ = \hat{\boldsymbol{x}}_k^- + K_k\left[\tilde{z}_k - h_k(\hat{\boldsymbol{x}}_k^-)\right] \tag{28a}$$
$$\mathcal{P}_k^+ = \left[I - K_k H_k(\hat{\boldsymbol{x}}_k^-)\right]\mathcal{P}_k^- \tag{28b}$$

where the superscript $(+)$ stands for the updated value and $(-)$ stands for the a priori value. The Kalman gain matrix is given by

$$K_k = \mathcal{P}_k^- H_k(\hat{\boldsymbol{x}}_k^-)^T\left[H_k(\hat{\boldsymbol{x}}_k^-)\mathcal{P}_k^- H_k(\hat{\boldsymbol{x}}_k^-)^T + R_k\right]^{-1} \tag{29}$$

where $H_k(\hat{\boldsymbol{x}}^-)$ is the measurement sensitivity matrix, given by

$$H_k(\hat{\boldsymbol{x}}_k^-) = \left.\frac{\partial h_k(\boldsymbol{x}(t_k)^-)}{\partial \boldsymbol{x}(t_k)}\right|_{\boldsymbol{x}=\hat{\boldsymbol{x}}} \tag{30}$$
$$= \begin{bmatrix} 1 & 0 \end{bmatrix}$$

Thus with the use of the internal pressure measurements the EKF algorithm can be used to estimate the leak hole area. Then the magnitude of vent thrust can be calculated by substituting the estimated values of $\hat{P}$ and $\hat{A}$ into Eq. (11).

UNSCENTED FILTER

An unscented filtering approach is considered here as an alternative to the EKF for the attitude and angular rate estimation of the ISS. The Unscented Filter (UF) has first been proposed by Julier and Uhlman in 3. Unlike the EKF, the UF captures the posterior mean and covariance of a random variable accurately to the second-order Taylor series expansion for any nonlinearity by choosing a minimal set of sample points and propagating them through the original nonlinear system. Also it is derivative-free, i.e. no Jacobian and Hessian calculations need to be evaluated for the computation. Therefore it can be easily applied to any complex dynamical system and to non-differentiable functions.[4] A detailed description of the error performance of the UF over EKF can be found in Refs. 3, 4 and 10. The general formulation of the UF in discrete-time is described here.

Let the discrete-time nonlinear system and observation model be

$$\boldsymbol{x}_{k+1} = \boldsymbol{f}\left(\boldsymbol{x}_k, \boldsymbol{u}_k, \boldsymbol{w}_k, k\right) \tag{31a}$$

$$\tilde{\boldsymbol{y}}_{k+1} = \boldsymbol{h}\left(\boldsymbol{x}_{k+1}, \boldsymbol{u}_{k+1}, k+1\right) + \boldsymbol{v}_{k+1} \tag{31b}$$

where $\boldsymbol{x}_{k+1}$ and $\boldsymbol{y}_{k+1}$ is an n dimensional state vector and observation vector respectively, $\boldsymbol{f}$ and $\boldsymbol{h}$ are the nonlinear models, $\boldsymbol{u}_k$ is a deterministic input. The vectors $\boldsymbol{w}_k$ and $\boldsymbol{v}_{k+1}$ are zero-mean Gaussian process and measurement noise with covariances Q_k and R_k respectively. Using a numerical integration scheme, a continuous-time system model can always be expressed in the discrete-time model. In the EKF problems arise because the predictions are approximated simply as functions of the previous state estimates:

$$\hat{\boldsymbol{x}}_{k+1}^{-} = E\left[\boldsymbol{f}\left(\boldsymbol{x}_k, \boldsymbol{u}_k, k\right)\right] \approx \boldsymbol{f}\left(\hat{\boldsymbol{x}}_k, \boldsymbol{u}_k, k\right) \tag{32}$$

$$\hat{\boldsymbol{y}}_{k+1} = E\left[\boldsymbol{h}\left(\boldsymbol{x}_k, \boldsymbol{u}_k, k\right)\right] \approx \boldsymbol{h}\left(\hat{\boldsymbol{x}}_k, \boldsymbol{u}_k, k\right) \tag{33}$$

But if the estimated state is nearby the true value, then the filter usually has a good convergence.

The UF state and error covariance updates are given as

$$\hat{\boldsymbol{x}}_k^{+} = \hat{\boldsymbol{x}}_k^{-} + K_k \boldsymbol{v}_k \tag{34}$$

$$\boldsymbol{v}_k = \tilde{\boldsymbol{y}}_k - \hat{\boldsymbol{y}}_k^{-} = \tilde{\boldsymbol{y}}_k - \boldsymbol{h}\left(\hat{\boldsymbol{x}}_k^{-}, \boldsymbol{u}_k, k\right) \tag{35}$$

$$P_k^{+} = P_k^{-} - K_k P_k^{vv} K_k^T \tag{36}$$

$$K_k = P_k^{xy}\left(P_k^{vv}\right)^{-1} \tag{37}$$

where $\boldsymbol{v}_k$ is the innovation and P_k^{vv} is the covariance of $\boldsymbol{v}_k$. The filter gain is K_k and P_k^{xy} is the cross-correlation matrix between $\hat{\boldsymbol{x}}_k^{-}$ and $\hat{\boldsymbol{y}}_k^{-}$. One of the way to deal with the process noise is to augment the covariance matrix with[10]

$$P_k^a = \begin{bmatrix} P_k^{+} & P_k^{xw} \\ \left(P_k^{xw}\right)^T & Q_K \end{bmatrix} \tag{38}$$

where P_k^{xw} is the correlation between the state and the process noise. The assumption is made here that the measurement noise $\boldsymbol{v}$ is purely addictive unlike the process noise. The set of $2L(=4n)$ σ points are computed as follows:

$$\boldsymbol{\sigma}_k\left(i\right) = \pm\sqrt{\left(L+\lambda\right)\left[P_k^a\right]_i} \quad \text{where } i = 1, 2, \ldots, L \tag{39}$$

where λ is the weighting factor which scales the distribution of the points. The vector $\sqrt{\left(L+\lambda\right)\left[P_k^a\right]_i}$ represents i^{th} column of the matrix square-root $\sqrt{\left(L+\lambda\right)\left[P_k^a\right]}$. The matrix square-root can be calculated directly by a lower triangular Cholesky factorization method.

These $\boldsymbol{\sigma}_k\left(i\right)$ points translate the mean $\hat{\boldsymbol{x}}_k^a$ as

$$\boldsymbol{\chi}\left(0\right) = \hat{\boldsymbol{x}}_k^a, \quad \boldsymbol{\chi}\left(i\right) = \hat{\boldsymbol{x}}_k^a + \boldsymbol{\sigma}_k\left(i\right) \tag{40}$$

where $\hat{\boldsymbol{x}}_k^a$ is an augmented state defined as

$$\boldsymbol{x}_k^a = \begin{bmatrix} \boldsymbol{x}_k \\ \boldsymbol{w}_k \end{bmatrix}, \quad \hat{\boldsymbol{x}}_k^a = \begin{bmatrix} \hat{\boldsymbol{x}}_k \\ \boldsymbol{0}_n \end{bmatrix} \tag{41}$$

The transformed set of χ points are propagated to $k+1$ for each of the $2L+1$ points by

$$\boldsymbol{\chi}_{k+1}\left(0\right) = \boldsymbol{f}\left(\boldsymbol{\chi}_k\left(0\right), \boldsymbol{u}_k, k\right), \quad \boldsymbol{\chi}_{k+1}\left(i\right) = \boldsymbol{f}\left(\boldsymbol{\chi}_k\left(i\right), \boldsymbol{u}_k, k\right) \tag{42}$$

The predicted mean is

$$\hat{\boldsymbol{x}}_{k+1}^{-} = \frac{1}{L+\lambda}\left\{\lambda\boldsymbol{\chi}_{k+1}^x\left(0\right) + \frac{1}{2}\sum_{i=1}^{2L}\boldsymbol{\chi}_{k+1}^x\left(i\right)\right\} \tag{43}$$

where $\boldsymbol{\chi}^x$ is a vector of the first n elements of $\boldsymbol{\chi}^a$. The predicted covariance is

$$P_{k+1}^{-} = \frac{1}{L+\lambda}\left\{\lambda\left[\boldsymbol{\chi}_{k+1}^x\left(0\right) - \hat{\boldsymbol{x}}_{k+1}^{-}\right]\left[\boldsymbol{\chi}_{k+1}^x\left(0\right) - \hat{\boldsymbol{x}}_{k+1}^{-}\right]^T + \frac{1}{2}\sum_{i=1}^{2L}\left[\boldsymbol{\chi}_{k+1}^x\left(i\right) - \hat{\boldsymbol{x}}_{k+1}^{-}\right]\left[\boldsymbol{\chi}_{k+1}^x\left(i\right) - \hat{\boldsymbol{x}}_{k+1}^{-}\right]^T\right\} \tag{44}$$

The predicted observation is calculated as

$$\hat{\boldsymbol{y}}_{k+1}^{-} = \frac{1}{L+\lambda}\left\{\lambda\boldsymbol{\gamma}_{k+1}\left(0\right) + \frac{1}{2}\sum_{i=1}^{2L}\boldsymbol{\gamma}_{k+1}\left(i\right)\right\} \tag{45}$$

where

$$\boldsymbol{\gamma}_{k+1}\left(i\right) = \boldsymbol{h}\left(\boldsymbol{\chi}_{k+1}^x\left(i\right), \boldsymbol{u}_{k+1}, k+1\right) \tag{46}$$

The output covariance is given by

$$P_{k+1}^{yy} = \frac{1}{L+\lambda}\left\{\lambda\left[\boldsymbol{\gamma}_{k+1}\left(0\right) - \hat{\boldsymbol{y}}_{k+1}^{-}\right]\left[\boldsymbol{\gamma}_{k+1}\left(0\right) - \hat{\boldsymbol{y}}_{k+1}^{-}\right]^T + \frac{1}{2}\sum_{i=1}^{2L}\left[\boldsymbol{\gamma}_{k+1}\left(i\right) - \hat{\boldsymbol{y}}_{k+1}^{-}\right]\left[\boldsymbol{\gamma}_{k+1}\left(i\right) - \hat{\boldsymbol{y}}_{k+1}^{-}\right]^T\right\} \tag{47}$$

then the innovation covariance is given by

$$P_{k+1}^{vv} = P_{k+1}^{yy} + R_{k+1} \tag{48}$$

Finally the cross correlation matrix is

$$P_{k+1}^{xy} = \frac{1}{L+\lambda}\left\{\lambda\left[\boldsymbol{\chi}_{k+1}^{x}(0) - \hat{\boldsymbol{x}}_{k+1}^{-}\right]\left[\boldsymbol{\gamma}_{k+1}(0) - \hat{\boldsymbol{y}}_{k+1}^{-}\right]^{T} + \frac{1}{2}\sum_{i=1}^{2L}\left[\boldsymbol{\chi}_{k+1}^{x}(i) - \hat{\boldsymbol{x}}_{k+1}^{-}\right]\left[\boldsymbol{\gamma}_{k+1}(i) - \hat{\boldsymbol{y}}_{k+1}^{-}\right]^{T}\right\} \tag{49}$$

The filter gain, the state and error covariance update is then computed using Eqs. (34) and (37). The weight λ can be chosen as $\lambda = 3 - L$ if the state $\boldsymbol{x}$ is assumed to belong to the Gaussian distribution.[11] Although λ can be either positive or negative, the negative values may lead to a non-positive semi-definite covariance matrix.

The UF is used in attitude, vent torque, and inertia matrix estimation in our leak localization algorithm. For the attitude estimation, the Unscented Quaternion Estimator (USQUE) developed by Crassidis and Markley has been implemented. For further details on USQUE, refer Ref. 12.

DISTURBANCE TORQUE ESTIMATION

The vent torque, which is not explicitly modeled in the attitude dynamics, shows up as a residual disturbance torque when the spacecraft angular rate measurement undergoes a filtering process. In the disturbance torque estimation algorithm, the filter state vector is augmented to include the unknown parameters as additional states, resulting in a total of 6 filter states, where 3 states are for the angular rate or angular momentum of the spacecraft and the rest 3 states are for the 3-axis components of the disturbance torque. Note that the attitude quaternion, which is needed to determine the gravity-gradient and aerodynamic torque in the disturbance torque estimation algorithm, is estimated separately by the USQUE method described in the previous section. In this section the disturbance estimation algorithm using the UF approach is shown.

The state system model for the torque estimation filter with $\boldsymbol{x} = [\boldsymbol{H},\ \boldsymbol{d}_{vent}]^T$ can be expressed as

$$\begin{bmatrix} \dot{\boldsymbol{H}} \\ \dot{\boldsymbol{d}}_{vent} \end{bmatrix} = \begin{bmatrix} \boldsymbol{f}_H(\boldsymbol{H}, \boldsymbol{d}_{vent}) \\ \boldsymbol{f}_d(\boldsymbol{H}, \boldsymbol{d}_{vent}) \end{bmatrix} + \begin{bmatrix} \boldsymbol{\eta}_H \\ \boldsymbol{\eta}_d \end{bmatrix}$$

$$= \begin{bmatrix} -J^{-1}(\boldsymbol{H} - \boldsymbol{h}) \times \boldsymbol{H} + \boldsymbol{L} + \boldsymbol{d}_{vent} \\ \boldsymbol{0}_{3\times 1} \end{bmatrix} + \begin{bmatrix} \boldsymbol{\eta}_H \\ \boldsymbol{\eta}_d \end{bmatrix} \tag{50}$$

where $\boldsymbol{d}_{vent}$ is the vent disturbance torque, $\boldsymbol{\eta}_H$ and $\boldsymbol{\eta}_d$ are zero-mean Gaussian process noises which correspond roughly to the possible range of the disturbance variations. The quantity $\boldsymbol{L}$ is the external disturbance torque vector which can be expressed as

$$\boldsymbol{L} = \boldsymbol{N}_{drag} + \boldsymbol{N}_{grav} \tag{51}$$

The quantity $\boldsymbol{L}$ is treated as a deterministic input in the filter equations. Also the CMG control input $\boldsymbol{h}$ should be low pass filtered because of the presence of high-frequency noise when measuring the CMG wheel speed. Note that the vent torque $\boldsymbol{d}_{vent}$ is treated as a random walk process. The gyroscope output measurement model is

$$\begin{aligned} \tilde{\boldsymbol{y}} &= \boldsymbol{\omega} + \boldsymbol{\eta}_1 \\ &= J^{-1}(\boldsymbol{H} - \boldsymbol{h}) + \boldsymbol{\eta}_1 \end{aligned} \tag{52}$$

Unlike the EKF, the UF approach does not need any derivation of the Jacobian and the sensitivity matrices. For the UF we need only the original nonlinear equation and measurement model. In the disturbance estimation algorithm, the UF approach may be especially more robust than the EKF because the initial conditions for the angular rate components may be fairly accurate within the uncertainties of the gyroscope, but the initial guess of the disturbance torque, which is not measured, may be far from the true value.

Numerical simulations for the UF cases are performed with the angular rate noise standard deviation of 2.3×10^{-4} °/sec ($\sigma_1 = 4 \times 10^{-6}$ rad/sec) and the sampling frequency of 1 Hz for the ISS assembly stage UF1. It is as-

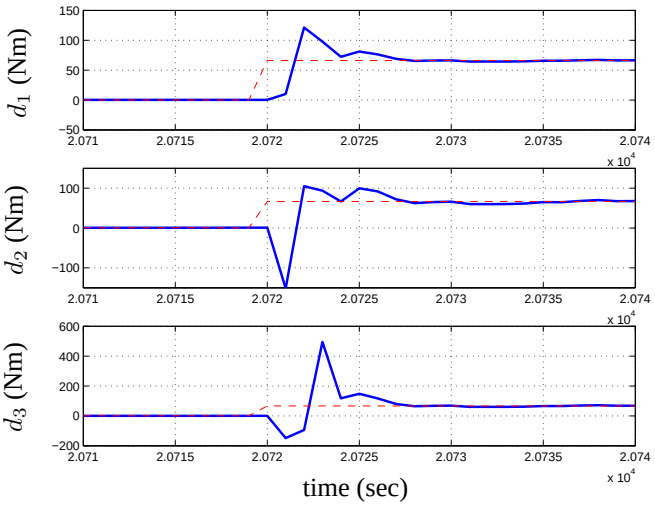

Fig. 4 Vent Torque Estimate Using UF with True Value

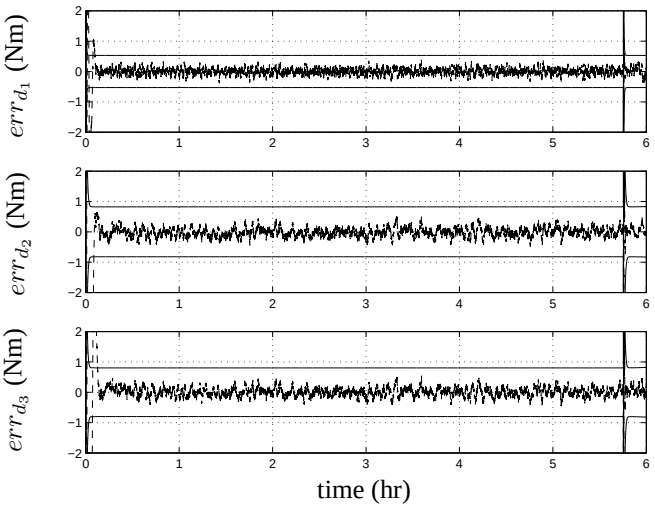

Fig. 5 Disturbance Torque Estimation Error Using UF

sumed that the spacecraft attitude is maintaining the TEA when suddenly after 5.7556 hr (20720 sec) a vent torque of 66.07 Nm is applied in each body axis of the spacecraft. The disturbance torque estimate results after the vent are shown in Fig. 4, where the dashed lines correspond to the true values. We can see that the vent torque estimates converge to the true values around 10 seconds after the leak. When an air leak occurs, the state covariance of the filter is reset to a large value to incorporate the variation of the disturbance torque at the instant when leak occurs (remember that we know when leak occurs by sensing the air depress inside the crew cabin). In this way the filter converges much faster than that of the filter algorithm without a covariance reset. The estimation errors for each component of the disturbance torque are shown in Fig. 5 with their 3σ-bound lines.

INERTIA ESTIMATION

For the ISS, the uncertainty in the aerodynamic torque may affect the vent torque estimation results if they have the same order of magnitude with the torque due to a leak. But the major uncertainty in the residual torque estimation is likely caused by the inaccurate ISS inertia mass components. For the ISS, the inertia of each configuration is pre-calculated on ground with CAD tools. But these values may not be precise since the ISS is made up of multiple complex rigid bodies interconnected to each other and undergoes several configuration changes during its lifetime.

Therefore, online parameter estimation method may be employed to estimate these slowly changing inertia in real-time when we know that there is no venting leak acting on the spacecraft. But the parameter estimation performance depends heavily on the observability of the parameters of interest. Usually in the parameter estimation problem, the state vector is extended by adjoining it with the vector of unknown parameters, as we have done for the vent torque estimation algorithm. In this section, we use the least-square approach to analyze the relative observability of the ISS inertia components.

When the ISS attitude is near the LVLH, the inertia matrix are unobservable even though there are some slight attitude variations due to the time varying aerodynamic torque. Assuming that the aerodynamic parameters are known, the inertia matrix observability in an ideal LVLH fixed mode can be shown from the following equations:

$$
\begin{aligned}
J_{23} &= \frac{1}{4n^2}(\tau_{aero\,1} - u_1) \\
J_{13} &= \frac{1}{3n^2}(u_2 - \tau_{aero\,2}) \\
J_{12} &= \frac{1}{n^2}(u_3 - \tau_{aero\,3})
\end{aligned} \tag{53}
$$

where the constant angular rate $\boldsymbol{\omega} = [0 \; -n \quad 0]^T$ and the constant attitude quaternion $\boldsymbol{q} = [0\;0\;0\;1]^T$ are substituted in the rotational Euler equations of motion. The quantities $\tau_{aero\,i}$ and u_i are the i^{th} component of the aerodynamic torque and the control torque input, respectively, and J_{ij} is the ij^{th} inertia matrix element. The spacecraft is assumed to be rotating in an Earth-pointing mode with a constant attitude angular rate $n = 0.0011$ rad/sec. We can see from Eqs. (53) that among the six inertia components, only the products of inertia (J_{23}, J_{13} and J_{12}) show up due to the presence of the gravity-gradient torque. But note that the control input $\boldsymbol{u}$ and the aerodynamic torque $\boldsymbol{\tau}_{aero}$ have small values with the same order of magnitude. Therefore, exact knowledge of the aerodynamic and control input torque are needed to directly calculate the product of inertias, which is not feasible in a real world.

A numerical test is done with the batch least-square method to check the observability conditions in the LVLH fixed attitude mode. The assumptions are: 1) perfect measurements of the attitude, angular rate, control input and the angular acceleration are available, 2) perfect knowledge of the aerodynamic torque, 3) no other disturbances besides aerodynamic and gravity-gradient torque are present. The solution of the least-square method for the estimation of the inertia matrix is as follows:

$$
\hat{\boldsymbol{x}} = (H^T H)^{-1} H^T \tilde{\boldsymbol{y}} \tag{54}
$$

where $\hat{\boldsymbol{x}}$ is a 6-dimensional vector containing the elements of the inertia matrix as

$$
\hat{\boldsymbol{x}} = \underline{\boldsymbol{J}} = [J_{11}\; J_{22}\; J_{33}\; J_{23}\; J_{13}\; J_{12}]^T \tag{55}
$$

and the H and the $\tilde{\boldsymbol{y}}$ are quantities known from the measurements and the control inputs. Note that a linear parametrization of the equations of motion is needed to use the batch least-square method. The Euler equations can be linearly parameterized with respect to the unknown inertia components as

$$
\begin{aligned}
-\boldsymbol{u} + \boldsymbol{\tau}_{aero} = &\quad J\dot{\boldsymbol{\omega}} + \boldsymbol{\omega} \times J\boldsymbol{\omega} - 3n^2 \boldsymbol{C}_3 \times J\boldsymbol{C}_3 \\
= &\quad [D_1(\dot{\boldsymbol{\omega}}) + D_3(\boldsymbol{\omega}) - 3n^2 D_3(\boldsymbol{C}_3)]\underline{\boldsymbol{J}} \\
\tilde{\boldsymbol{y}} = &\quad H\underline{\boldsymbol{J}}
\end{aligned} \tag{56}
$$

where the matrices D_1 and D_3 are defined as in 6.

The quantity $H^T H$ should be strictly positive definite since its inverse appears in Eq. (54) to solve the unknown parameters $\hat{\boldsymbol{x}}$. In practice, we require $H^T H$ to be well-conditioned, a useful measure of the condition of a matrix is the condition number. The condition number varies from 1 for an orthogonal matrix to infinity for a singular matrix. From a numerical simulation, when all six components of inertia matrix are solved using the Eq. (54), the condition number of the $H^T H$ is 1.7×10^{10} resulting in the divergence of the solution. The relative observability among the inertia components is analyzed using the eigenvalue and eigenvector decomposition of the $H^T H$ matrix, which is shown in Fig. 6. In this figure we can see the relative observability of the inertia components. For example, J_{11} is the maximum component of the eigenvector which corresponds to the eigenvalue around 10^{-15}. As expected the three products of inertia, which have their eigenvalues near 10^{-6} are the most observable components among the elements, whereas the three moments of inertia have their

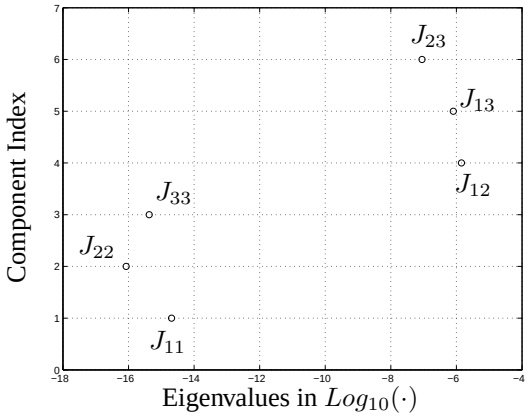

Fig. 6 Relative Observability of Inertia

magnitude near 10^{-15} which is 10^{-9} smaller than those of the products of inertia. A simulation has been done to estimate the product of inertia with a batch least-square method, and the results are shown in Fig. 7 (where the results are calculated at regular instant of time with the cumulative measurements). The three components con-

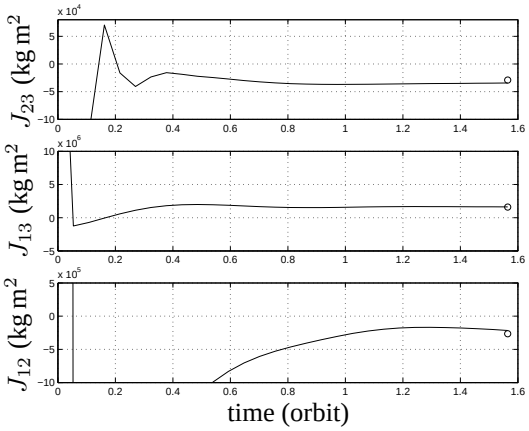

Fig. 7 Inertia Product Estimates Using Least-Square Method

verge very fast within an orbit to its true values as expected. The corresponding condition number is 16 which is much smaller than the previous simulation case revealing that the $H^T H$ is now a well-conditioned matrix. But note that the presence of noise in the measurements makes the products of inertia unobservable. For the real-time estimation of the inertia, the UF approach is used because of its robustness in the presence of large initial state uncertainty. Also, the inertia estimation should be performed only when an attitude maneuver is present to enhance the observability of the parameters.

LEAK LOCALIZATION

Once a vent torque $\boldsymbol{d}_{vent}$ is estimated by the real-time filter, the next step involves determining the position vector $\boldsymbol{r}_{vent}$, which is the moment arm of the vent torque satisfying

$$\boldsymbol{d}_{vent} = \boldsymbol{r}_{vent} \times \boldsymbol{F}_{vent} \tag{57}$$

In the above equation, the vent torque $\boldsymbol{d}_{vent}$ and the magnitude of $\boldsymbol{F}_{vent}$ are known by the estimation algorithms. The overall steps for locating a leak on the ISS are as follows:

1. Model the 3 dimensional geometric surfaces of the pressurized parts of the spacecraft.
2. Estimate the vent torque and magnitude of the vent thrust.
3. Slice the 3-D surfaces of the pressurized modules with a plane perpendicular to the direction of the vent torque so that this plane comprises the center of mass of the spacecraft. From the fundamental definition of torque, a torque about the center of mass of a rigid body is perpendicular to the plane comprising the vectors $\boldsymbol{r}_{vent}$ and $\boldsymbol{F}_{vent}$. So, $\boldsymbol{r}_{vent}$, $\boldsymbol{F}_{vent}$ and the center of mass are all in the same plane normal to the direction of the vent torque. Denote this plane by τ. The intersection between the plane τ and the surface of the spacecraft produces contours.
4. With the assumption that the vent thrust is normal to the tangent plane of the partial section on the ISS surface where the leak occurs, calculate the gradient vectors (direction normal vectors) of the points that make up the sliced contours obtained in Step 3.
5. Multiply the magnitude of the vent thrust estimated in Step 1 with all gradient vectors calculated in Step 4.
6. Since the position and gradient vectors of all the points making the sliced contours are known, calculate the resulting torque at each point on the contours.
7. From the torques obtained for each point in Step 6, select the torques that are closest to the estimated torque (within an error bound) and check their points on the contours.

The actual geometric structure of the station eliminates many of the possible solutions; however, multiple solutions may still exist. In this case further assumptions can be made, such as the probability of impacts by the debris or small meteorites is low on the aft and nadir facing surfaces since these surfaces are shaded by other structures. Also, the leak localization method based on the attitude response may be combined with the conventional leak localization methods. For example, if the solution shows two leaks situated at two different modules then only one hatch closure between any of these modules is needed to check which one of the two modules leaks. Furthermore, visual inspections by the crew may narrow the possible leak solutions.

NUMERICAL SIMULATION

A user-friendly design tool coded entirely in MATLAB has been developed to estimate a leak location under various conditions. The tool supports several ISS assembly stages from 11A to UF-7 but it may need to be modified due to the uncertainties in the future of the ISS program. The 3-D surface models of the pressurized segment of the ISS Stage have been developed based on the data provided in Ref. 1. Figures 8 and 9 show the main Graphical User Interfaces (GUIs) of the tool. Users can input the orbit, the mass and the aerodynamic parameters of the ISS, and choose a simulated leak location with the GUI shown in Fig. 8. The resulting leak locations after the leak localiza-

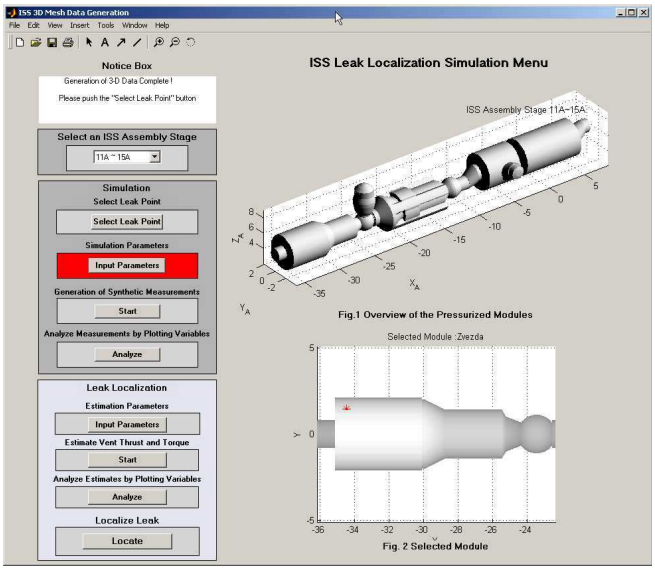

Fig. 8 GUI for Simulation of the Leak Localization Algorithm

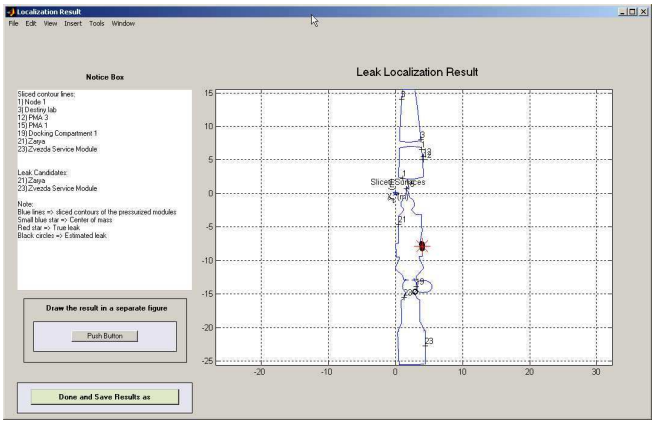

Fig. 9 GUI for Leak Localization Results

tion estimation process will be shown on the GUI shown in Fig. 9.

For the simulation, the ISS assembly Stage 16A is considered (see Fig. 10). The isentropic depressurization process of the air inside the ISS is assumed. The mass and aerodynamic properties of the ISS are provided in Ref. 1. The inertia J is given by

$$J = \begin{bmatrix} 127908568 & 3141229 & 7709108 \\ 3141229 & 107362480 & 1345279 \\ 7709108 & 1345279 & 200432320 \end{bmatrix} \text{(kg m)}^2 \tag{58}$$

The centers of pressure are $\boldsymbol{\rho}_{cpx} = [0, -0.355, -0.927]^T$ m, $\boldsymbol{\rho}_{cpy} = [-7.94,\ 0, -1.1]^T$ m and $\boldsymbol{\rho}_{cpz} = [1.12,\ 0.247,\ 0]^T$ m in the Space Station Analysis Coordinate System (SSACS) with respect to the center of mass. The components x, y and z represent the three orthogonal axes of the ISS body fixed frame.[1] The reference projected areas are $S_x = 967$ m^2, $S_y = 799$ m^2 and $S_z = 3525$ m^2.

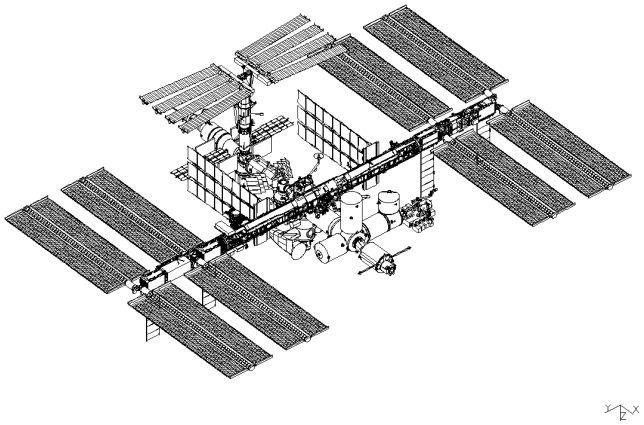

Fig. 10 ISS Assembly Stage 16A

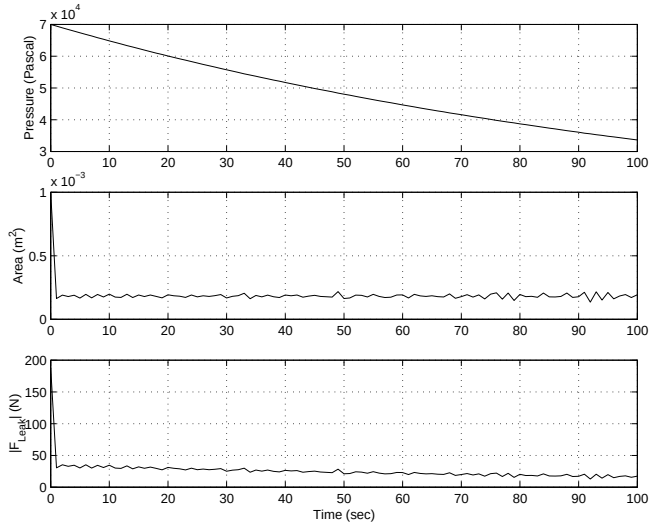

Fig. 11 Vent Thrust Magnitude and Hole Area Estimate

The Global Positioning System (GPS) attitude-sensor measurement-error standard deviation is given by $\sigma_q = 0.5$ deg, and the ring-laser gyro sensor measurement-error standard deviation is given by $\sigma_\omega = 4 \times 10^{-6}$ deg/sec.[13] The measurement-error standard deviation of the internal pressure is given by $\sigma = 0.1$ mmHg. For the depressurization of the air inside, the initial internal temperature and pressure are set to $T_0 = 21^o$ C and $P_0 = 1$ atm, respectively. The back pressure is assumed to be $P_B = 0$ atm, and the volume of the entire pressurized system for ISS 16A is $V = 867.2$ m^3. Finally, an inertia uncertainty of 3% is added to the true J.

Simulations are done for 100 seconds from the start of the leak. Figure 11 shows the estimate of the leak hole area using the Kalman filter algorithm. The true leak hole area A is 1.8241×10^{-4} m^2. As seen from this figure the Kalman filter accurately estimates the leak hole area. The vent thrust magnitude is then computed with the internal pressure measurement and the estimate of the hole area.

For the first simulation, a leak is assumed on a module shown in Fig. 12. The sliced plane τ with contours in 3-D

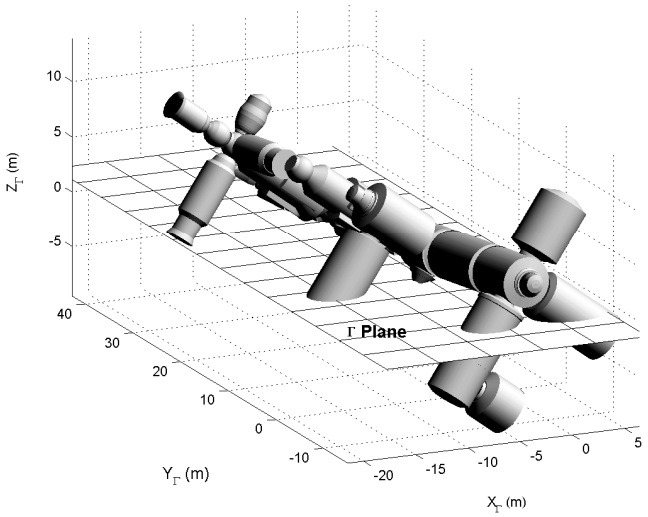

Fig. 12 Slicing 3-D Surface Model with Plane τ

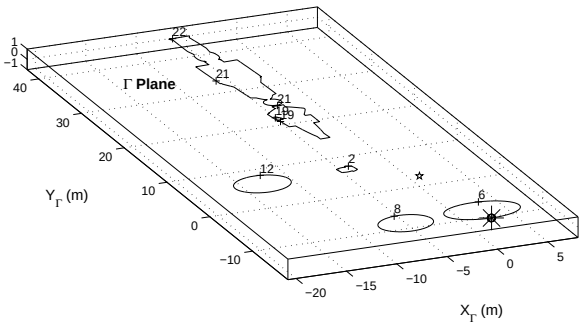

Fig. 13 Sliced Plane τ with Contours in 3-D

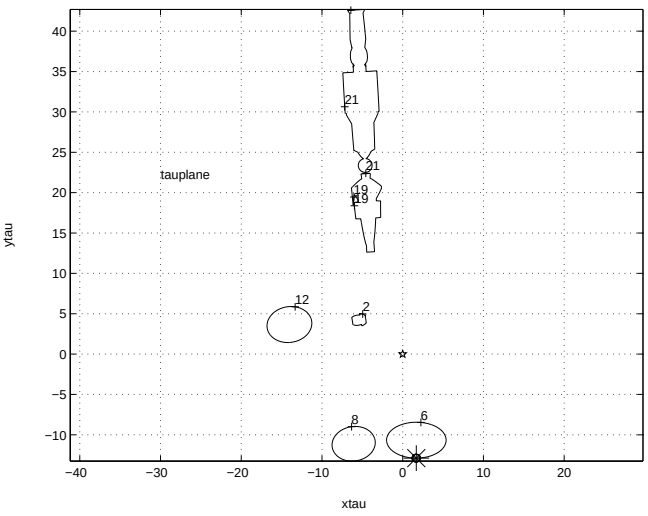

Fig. 14 Contours on Plane τ with Possible Leak

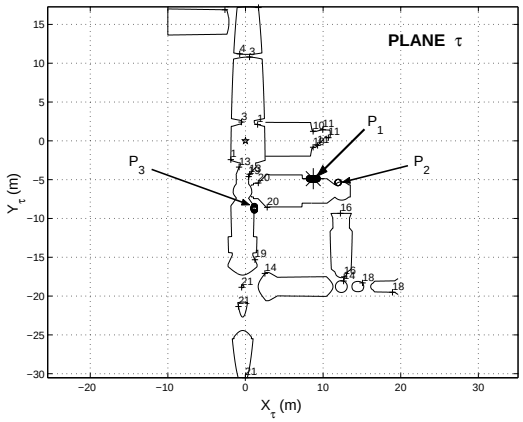

Fig. 15 Contours on Plane τ with 3 Possible Leaks

is shown in Fig. 13. Using the leak localization approach a single leak has been determined for this simulated case, depicted in Fig. 14. The estimated position is marked with a $\circ$, the true position of a leak is marked with a $*$ for comparison, and the center of mass is marked with a $\star$ on the plane τ. Slicing of the 3-D surface is performed at the end of the simulation ($t = 100$ sec). If no errors are present in the assumed model and if the assumptions made so far are perfectly satisfied, then the closest torque yielding the point to the estimated vent torque is the true leak point. But because of sensor inaccuracies and modelling errors in the inertia, the estimated vent torque may deviate from the true value. Therefore, an upper error-bound should be set when selecting points that yield the torque closest to the estimated vent torque. For the case shown in Fig. 14, we conclude that the leak occurs on the contour line labelled 8, which corresponds to the Kibo JEM pressurized module. In this simulated case, the leak location is well estimated using the new localization method.

Another simulation has been done where multiple locations may result from the given estimated vent torque. In this case the estimated leak locations are spread over several modules, as shown in Fig. 15. The locations P_1, P_2 and P_3 are possible leak candidates (the true leak point is situated near P_1). But since P_1 and P_2 are on the same module, a crew person only needs to close one hatch between the module labelled 20 and the module labelled 19 to verify which one of the two modules has a leak. This is accomplished by measuring the internal pressure drop rate or using visual inspections of the estimated leak points. If the leak hole is due to space debris or small meteorite punctures, then the aft and nadir facing surfaces of the ISS have little possibility to be impacted. This is also true for locations where regions are protected by other structures, as is the case for point P_3. Therefore this point is not a likely candidate for the leak.

Initial results indicate that the leak localization method may be sensitive to modelling errors, such as the spacecraft mass properties and aerodynamic parameters. Also the effect of the disturbance torque caused by the pressure of the impingement of the leaking air plume on nearby surfaces

may be a critical source of disturbance when a leak occurs. Because of inherent complexities, analyzing these effects may be difficult. Experimental validation of the algorithm has been treated in Ref. 14.

CONCLUSIONS

In this paper a new leak localization method using the attitude response is developed for the ISS. The reaction thrust arising from a vent due to air leak are calculated using the isentropic nozzle theory. Also, the isentropic and isothermal depressurization models have been considered to describe the depressurization process of the pressurized module. Based on these models, the vent thrust magnitude is estimated by employing the KF. The UF approach is used for the purpose of estimating the attitude and residual disturbance torque. The UF approach is preferred over the EKF since the expected error is lower and it avoids the derivation of complicated Jacobian matrices.

In the ISS, an incorrect inertia may be the primary source of uncertainty in estimating the vent torque. Also, unlike the deterministic gravity-gradient, the precise determination of the aerodynamic torque is very difficult due to the lack of the knowledge of the drag mechanism in rarefied atmosphere activities. But since the upper bound of the aerodynamic torque is known, the vent torque which is much larger than the aerodynamic torque has no much effect on the vent torque estimation results. It has been shown with the batch least-square analysis that the inertia matrix is unobservable when the ISS is near the LVLH. Therefore, to enhance the observability of the unknown parameters, an appropriate attitude maneuver should be performed. For the real-time inertia parameter estimation, the robustness in the presence of large initial state uncertainty and no necessities of the Jacobian derivations may make the UF approach attractive.

The actual geometric structure of the station eliminates many of the possible solutions; however, multiple solutions may still exist. In this case further assumptions should be made, such as the probability of impacts by the debris or small meteorites is low on the aft, nadir facing surfaces and some parts of the surfaces which is not likely to have leak. Also, the leak localization method based on the attitude response may be combined with the conventional leak localization methods. For example, if the solution shows two leaks situated at two different modules then only one hatch closure between any of these modules is needed to check which one of the two modules leaks. Furthermore, visual inspections by the crew may narrow the possible leak solutions.

Numerical results showed that the proposed leak localization method determines the location of the leak rapidly and precisely. Furthermore, actual test data from a depressurization of the Space Shuttle airlock indicates that the proposed method has the potential to accurately estimate the leak hole size and venting force magnitude.

The advantages of this localization method are: no other devices are needed besides pressure gauges, spacecraft attitude and rate sensors, and relatively fast leak localization can be achieved compared to the conventional leak localization method proposed for the ISS. Also this localization method not only determines the possible leaking modules but also the possible locations of a leak hole within the surfaces of the modules, which may be critical to allow for repairs rather than sealing off the module or performing a station evacuation.

ACKNOWLEDGEMENTS

This work has been supported by a grant from United Space Alliance (contract number C00-00109). This support is greatly appreciated.

References

[1] *International Space Station On-Orbit Assembly, Modeling, and Mass Properties Databook: Design Analysis Cycle Assembly Sequence, JSC-26557, Revision J*, Lockheed Martin, Houston, TX, 1999.

[2] *Protecting the Space Station from Meteoroids and Orbital Debris*, National Research Council, Washington, DC, 1997.

[3] Julier, S. J., Uhlmann, J. K., and Durrant-Whyte, H. F., "A New Approach for Filtering Nonlinear Systems," *American Control Conference*, pp. 1628-1632, Seattle, WA, 1995.

[4] Wan, E. and van der Merwe, R., "The Unscented Kalman Filter for Nonlinear Estimation," *Proceedings of IEEE Symposium 2000*, pp. 153-158, Lake Louise, Alberta, Canada, Oct. 2000.

[5] Bishop, R. H., Paynter, S. J., and Sunkel, J. W., "Adaptive Control of Space Station During Nominal Operations with CMGs," *IEEE Conference on Decision and Control*, Brighton, England, Dec. 11-13 1991.

[6] Carter, M. T., *Real-Time Analysis of Mass Properties*, Dissertation, Texas A&M University, College Station, February 1999.

[7] Paynter, S. J., *Adaptive Control of the Space Station*, M.s. thesis, University of Texas, Austin, December 1992.

[8] Carter, M. T. and Vadali, S. R., "Parameter Identification for the International Space Station Using Nonlinear Momentum Management Control," *AIAA-97-3524*, August 1997.

[9] Sonntag, R. E., Borgnakke, C., and Wylen, G. J. V., *Fundamentals of Thermodynamics*, John Wiley & Sons, Inc., New York, 5th ed., 1998.

[10] Crassidis, J. L. and Junkins, J. L., *Optimal Estimation of Dynamical Systems*, CRC Press, Boca Raton, FL, 2004.

[11] Julier, S. and Uhlmann, J., "A New Extension of the Kalman Filter to Nonlinear Systems," *Int. Symp. Aerospace/Defense Sensing, Simul. and Controls*, Orlando, FL, 1997.

[12] Crassidis, J. L. and Markley, F. L., "Unscented Filtering for Spacecraft Attitude Estimation," *Journal of Guidance, Control, and Dynamics*, Vol. 26, No. 4, July-August 2003, pp. 536–537.

[13] *United States Control Module Guidance, Navigation, and Control Subsystem Design Concept*, NASA MSFC-3677, Huntsville, AL, March 1997.

[14] Kim, J. W., Crassidis, J. L., Vadali, S. R., and Dershowitz, A. L., "International Space Station Leak Localization Using Attitude Disturbance Estimation," Vol. 7, Aerospace Conference, Proceedings. 2003 IEEE, March 8-15 2003.